Water Oxidation

DOI: 10.1002/anie.201104367

High Photocurrent in Silicon Photoanodes Catalyzed by Iron Oxide Thin Films for Water Oxidation**

*Kimin Jun, Yun Seog Lee, Tonio Buonassisi, and Joseph M. Jacobson**

Solar water splitting is currently the subject of considerable attention as a potential inorganic path for renewable fuels. Although the product, hydrogen, can be applied directly as a fuel, a very promising direction is to use it as a key feedstock in the production of synthetic liquid fuels, such as those made by the Fischer–Tropsch method.[1] Solar water splitting is achieved by using a semiconductor cell to straddle the water redox potential thereby donating holes and electrons at the anode and cathode, respectively.[2,3] The anode reaction of conventional cells requires high overpotential owing to high-energy intermediate states,[4] which makes the development of efficient photoanodes an intense area of current research. Similar to solar-cell research, a key concern is to find candidate systems with optimal performance-to-cost ratios.

Silicon, with its good balance between low cost and narrow band gap matched to the visible solar spectrum, is widely used for photovoltaic applications, however its lack of catalytic functionality at the silicon–water interface coupled with a relatively high valence band edge position renders silicon a poor choice for use as a water-splitting photoanode. Attempts to overcome these problems in silicon have focused on heterojunction photoelectrodes,[5] and systems which separate photocurrent generation from electrolysis.[6] Unfortunately heterojunction systems suffer from poor performance to date and, in the case of electrolyzer systems, which lack the semiconductor–liquid junction, a large overpotential is needed because of the inability of these systems to take advantage of the built-in potential which comes from such an interface. Approaches to bypass the shortcomings of silicon altogether have involved the use of metal oxide films,[3,7] however these have suffered from poor carrier transport or wide band gap issues up until now.

Herein, we report high photocurrents from photoanodes composed of very thin iron oxide films on top of a silicon layer in a high pH value environment. Silicon plays the role of a primary light absorption layer while the iron oxide serves as a catalyst. The explicit application of iron oxide as a catalyst has been reported on metallic surfaces,[8] but with limited performance likely due to the poor transport properties of bulk films. Herein, we show that a sufficiently thin catalytic film allows for the presence of the silicon band structure to be present at the semiconductor–water interface while still providing for a catalytic water splitting surface. This arrangement allows for the production of particularly high photocurrents at the photoanode.

Figure 1 shows a scanning electron microscope (SEM) image and chemical characteristics of the iron oxide film deposited by chemical vapor deposition. This film was prepared from an iron precursor (iron pentacarbonyl) with a titanium dopant (titanium isopropoxide) for better activity.[9] Figure 1a illustrates an approximately 20 nm thick film, which required 10 minutes to deposit. X-ray photoelectron spectroscopy (XPS) measurements revealed 4% Ti composition. For dopant activation, high temperature (as high as 800 °C[10]) is required. However, our deposition temperature is lower than 200 °C, as a consequence, the active dopant level would be significantly lower than 4%. The magnified view around Fe 2p region (Figure 1b) shows $2p_{2/3}$ peak at 711 eV and a satellite peak at 719 eV, which are characteristics of Fe_2O_3.[11] From X-ray diffraction (XRD) result in Figure 1c, most of the peaks correspond to hematite (α-Fe_2O_3)[12] and the silicon substrate. Several unidentified peaks have full-width at half maximum (FWHM) values which are very narrow. Considering the polycrystalline nature of the thin iron oxide film, these peaks are believed to come from silicon.

For photocurrent measurements, devices were fabricated on n-type silicon, where an iron oxide film was deposited on the front, and a metal contact (aluminum/silver) and epoxy sealing was made on the back. A three-electrode photoelectrochemical cell was configured with electrolyte that consists of disodium hydrogen phosphate (Na_2HPO_4) and/or sodium hydroxide (NaOH) adjusted to desired pH value. A one-sun intensity (100 mW cm^{-2}) light flux was introduced, and all the electrode potentials were converted to reversible hydrogen electrode (RHE) potentials. All dark currents were omitted in the plots since they remained negligible throughout the swept voltage range (see Supporting Information, Figure S2).

Figure 2 shows the photoresponses varying two parameters, pH value (Figure 2a) and iron oxide film thickness (Figure 2b). At high pH value, the photoanodes with 10 minutes iron oxide deposition show current density of

[*] K. Jun, Y. S. Lee, T. Buonassisi, Prof. J. M. Jacobson
Department of Mechanical Engineering
Massachusetts Institute of Technology, Cambridge (USA)
K. Jun, Prof. J. M. Jacobson
The Center for Bits and Atoms, Media Laboratory, Massachusetts Institute of Technology
20 Ames street, E15-413, Cambridge, MA 02139 (USA)
E-mail: jacobson@media.mit.edu

[**] We acknowledge Kurt Broderick at the Microsystem Technology Laboratory, MIT for help with various fabrication processes. We also acknowledge Dr. Seungwoo Lee and Rupak Chakraborty at MIT for the electrochemical setup. This work was financially supported by MIT's Center for Bits and Atoms, the Chesonis Family Foundation, and an MIT Energy Initiative seed grant. K.J. was supported by the Samsung Scholarship Foundation.

Supporting information for this article is available on the WWW under http://dx.doi.org/10.1002/anie.201104367.

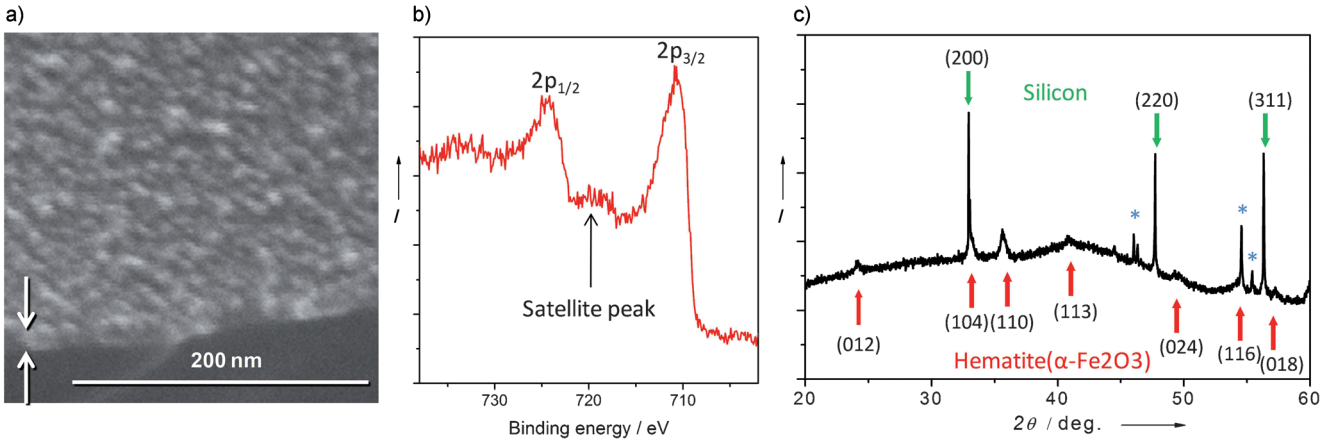

Figure 1. Characteristics of iron oxide films. a) SEM image of an iron oxide film deposited in 10 minutes; the film thickness is indicated by the arrow marks, b) section of the XPS spectrum around the Fe 2p energy region, c) XRD result, silicon peaks (green arrow) from substrate, hematite peaks (red arrow) from film, and unidentifiable peaks (blue asterisk).

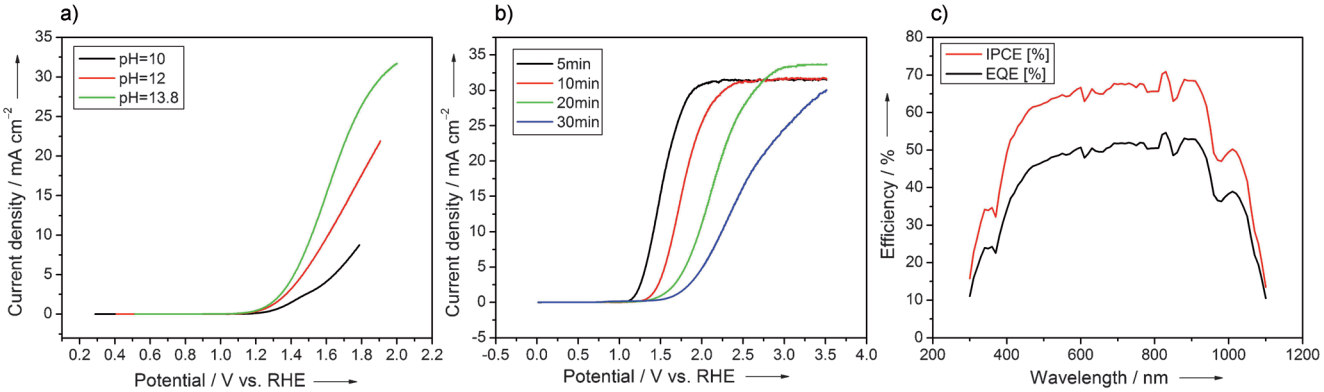

Figure 2. Parametric studies of photoresponse of iron oxide/silicon photoanodes. a) Photocurrent measurements at different pH values (10, 12, and 13.8) using a film deposited over 10 minutes, b) photocurrent with different film thickness (5, 10, 20, and 30 minutes deposition) at pH 13.8, c) external quantum efficiency (EQE) and incident photon to current efficiency (IPCE) using 10 minutes deposition film at 1.6 V vs. RHE and pH 12. RHE = reversible hydrogen electrode.

30–40 mA cm^{-2}, which is similar value of silicon solar cells, under low overpotential (Figure 2a). Considering there is no photoresponse in bare silicon (Supporting Information, Figure S4b) this strong activity is quantitatively as well as qualitatively impressive. Figure 2b demonstrates that thinner films have lower onset potentials than thicker films. Along with the incident photon to current efficiency (IPCE, see note S3) in Figure 2c which shows light absorption over a wide spectral range up to the silicon band gap energy of 1.12 eV ($\lambda = 1109$ nm), these observations suggest that the photocurrent arises from silicon rather than iron oxide film. Therefore, it is believed that, while light absorption and photocarrier generation occur within the silicon, the iron oxide layer plays a crucial catalytic role. Contributions to the high measured current from alternate sources including etching of silicon and iron oxide were ruled out by explicit consideration of the overall volume of semiconductor involved and any resultant valence charge contribution (see note S4 in the Supporting Information).

Although our results showed an abrupt current increase after the onset, the current density at 1.23 V vs. RHE (zero overpotential) was still low. Therefore it is necessary to lower the onset potential and to make the slope even steeper. One obvious loss comes from the Schottky contact between the silicon and the metal on the wafer backside. To eliminate this Schottky barrier, we formed a shallow n^+ doped-layer on the back side of the silicon by phosphorous spin-on dopant. After dopant diffusion, the sheet resistance reduced to 12–14 Ω sq^{-1}. Using devices made of this substrate, a current density of 12.2 mA cm^{-2} was obtained at 1.23 V vs. RHE and pH 13.8 (Figure 3a). Even at pH 12, which is a less destructive environment for silicon than pH 13.8, the current was still high, 4.34 mA cm^{-2}. Further improvement was made when a vertical array of silicon wires[13] was fabricated on this n^+ layered silicon, as shown in Figure 3b. Current densities of 17.27 mA cm^{-2} (pH 13.8) and 4.81 mA cm^{-2} (pH 12) were obtained at 1.23 V vs. RHE.

The anode reaction of water splitting (oxygen evolution) is challenging, since two water molecules should react with spatial coincidence through high-energy intermediate stages,[14] which necessitate good catalysts, such as noble metals and, more recently, cobalt[4] and nickel[15] compounds.

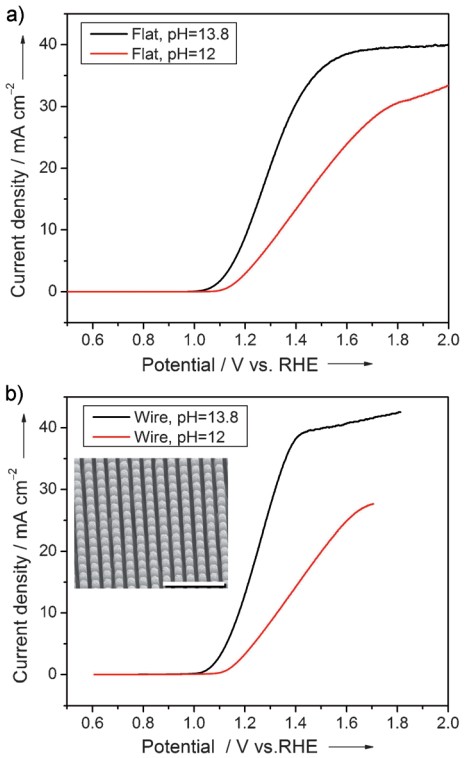

Figure 3. Optimization by silicon microfabrication techniques. a) Measured photocurrent of n^+ back-doped flat silicon at pH 12 and 13.8 with iron oxide deposited for 5 minutes, b) n^+ back-doped silicon wires array with 10 min iron oxide deposition at pH 12 and 13.8. Inset: SEM image of fabricated silicon wires array, scale bar 10 μm.

Since our device showed high reactivity after iron oxide catalysis, the catalytic functionality needs to be investigated. Figure 4 shows the current evolution by different catalysts (platinum and iron oxide) on indium tin oxide (ITO) substrates. Compared to bare ITO glass, both platinum and iron oxide are catalytic, but iron oxide performs better than platinum. Similar levels of iron oxide onset potential were reported elsewhere[16] in which the dark current onset is about 1.6–1.7 V vs. RHE, consistent with our observation.

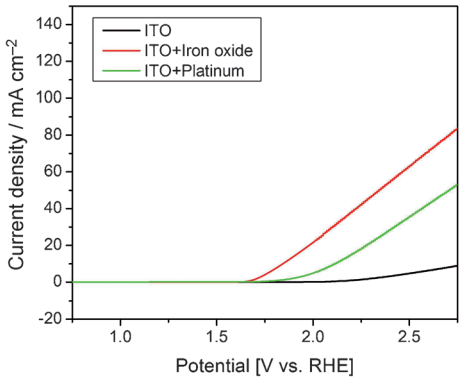

Figure 4. Catalytic effect comparison of bare ITO, platinum (5 nm) on ITO, and iron oxide film (10 minutes deposition) on ITO. All measurements at pH 13.8.

In addition to good catalytic functionality of thin iron oxide films, the favorable energy-band alignment of silicon contributes to the high photocurrent. Silicon is generally considered an unsuitable anode for water splitting because of its high valence band edge position. However, while most metal oxide semiconductors follow the Nernst relation[3,17] (i.e., flat band potential shifts −0.059 mV/pH), the silicon band potential is less sensitive to pH values. For example, Madou et al.[18] reported a −0.03 mV/pH value, varying slightly with chemical species and reactions. Therefore, at high pH values, the difference between the silicon valence band edge and oxygen evolution potential (OEP) would become small because the OEP also shifts by −0.059 mV/pH value. To verify our assumption, we measured the flat band potential of bare silicon (see Supporting Information, Figure S5), which is about −0.5 V vs. Ag/AgCl. Considering our wafer doping level (measured resistivity 22 Ω cm) and operation pH value (12–14), the valence band edge of silicon is below the OEP (see Supporting Information, Figure S6), which satisfies the energetic requirement for hole transfer. Nevertheless, spontaneous water oxidation cannot occur in bare silicon without catalytic assistance. In our case, the iron oxide seems to catalyze the oxidation reaction at the semiconductor–liquid junction.

Although α-Fe_2O_3 is a semiconductor, the approximately 10 nm thickness of our layers is thinner than the typical nondegenerate semiconductor space–charge region.[17] Since there is no metallic barrier between electrolyte and silicon, most of the space–charge region is within the silicon. Then, equilibrium induces a strong upward bending of the silicon energy band because the silicon flat band potential is negative (cathodic) with respect to OEP (Figure 5). This built-in potential, along with a good catalytic performance of iron oxide, is believed to be the reason for the high photocurrent in our silicon photoanode.

The flat band potential of bare silicon and silicon coated with a very thin (less than 10 nm) iron oxide film remain at a similar level (see Supporting Information, Figure S5). This result implies that the semiconductor characteristic of this

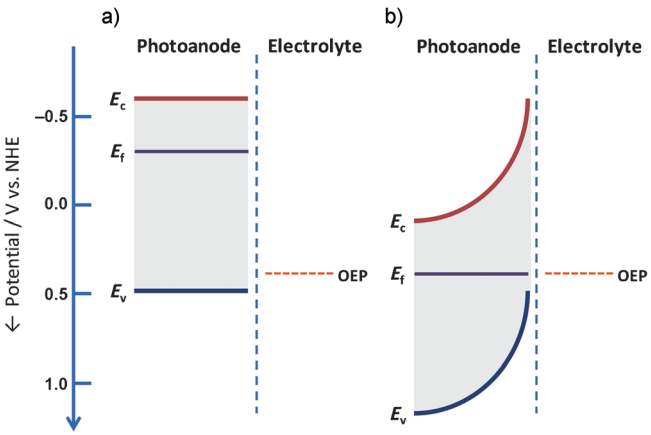

Figure 5. Energy band diagram at the interface between the silicon photoanode and the electrolyte. a) Flat band condition, b) equilibrium condition. NHE = normal hydrogen electrode. E_f = Fermi level, E_c = conduction band edge, E_v = valence band edge.

hybrid device is still governed by silicon. As the iron oxide gets thicker (over 20 nm), the flat band potential is shifted from that of bare silicon. This result shows that above this thickness the electronic characteristics of iron oxide are no longer negligible. Equivalent bulk resistance increases because of the short carrier diffusion length and low conductivity of iron oxide. Also, since the iron oxide now contributes to the potential drop, the built-in potential in the silicon decreases, which hampers the photoresponse as shown in Figure 2b. In spite of this analysis, the catalytic nature of iron oxide is still obscure. Therefore, further study is required to identify the unique physics at the silicon/iron oxide interface and at the iron oxide surface, which will aid in the search for improved oxygen-evolving catalysts.

Herein, we have demonstrated unprecedentedly high photocurrents in a water splitting anode reaction using a silicon-based photoelectrode. The combination of silicon and a very thin iron oxide film enables effective light absorption, photogenerated carrier separation, and oxygen-evolving catalysis. Considering the abundance of materials and the low technical barrier for manufacturing, this direction has the prospect of enabling an efficient solar-driven water-splitting pathway.

Experimental Section

Photoanode fabrication: Silicon electrodes were made of 4 inch (10 cm) n-type phosphorous-doped silicon wafers (resistivity 5–25 Ω cm, thickness 500–550 μm, (100) orientation) This wafer was diced into 1×1 cm^2 pieces that were cleaned in organic solvents and 1:10 hydrofluoric acid (HF, 49% wt., J. T. Baker): deionized water before chemical vapor deposition(CVD). The CVD setup (see Figure S1) is home built, comprising two bubblers and three mass-flow controllers (MFC, 1479A, MKS Instrument). At each bubbler, of iron pentacarbonyl ($[Fe(CO)_5]$, 10 mL; Sigma–Aldrich) and titanium isopropoxide ($[Ti\{OCH(CH_3)_2\}_4]$, 10 mL; Sigma–Aldrich) were contained. Iron pentacarbonyl was chilled in a cold water bath at 5 °C, and the titanium isopropoxide was maintained at room temperature (20 °C). 10 standard cubic centimeters per minute (sccm) argon and 250 sccm oxygen were fed into iron and titanium precursors, respectively. These two precursors and extra oxygen (350 sccm) was mixed and fed into a glass funnel (an enlarging adapter, 14/20 to 24/40). The silicon substrate was placed on a heated surface (ca. 173 °C), and the glass funnel was placed with 1 mm clearance from the surface. Film thickness was controlled by deposition time. All experiments were conducted at atmospheric pressure.

Device fabrication: The substrate backside was briefly (1 minute) cleaned with 1:10 HF:deioninzed water before metal deposition. Using a thermal evaporator, 7 nm aluminum, followed by 50 nm silver, was deposited. A silver wire with 0.5 mm diameter was attached to the metal contact by silver paint (silver in MIBK, Ted Pella) and dried for 30 minutes. Afterwards, the silver wire was insulated using Teflon tubing, and the backside was encapsulated with epoxy on slide glass. The epoxy was cured for more than 2 hours at 70 °C. To remove organic contaminants, the device was cleaned by ozone (Aqua-6 ozone generator, A2Z Ozone) for 10 minutes. Figure S1a shows the completed device.

Photocurrent measurement: Electrolytes were prepared with three different pH values. pH 13.8 was prepared by 1M sodium hydroxide (NaOH, Sigma–Aldrich) in deionized water (18 Ω cm). Lower pH values need only a tiny fraction of NaOH, but in this case, solution conductivity might be significantly lower than with 1M NaOH. To guarantee conductance, a buffer solution was prepared using 0.5M disodium hydrogen phosphate (Na_2HPO_4, Sigma–Aldrich), and titrated against an NaOH solution to make pH 12 and 10. This solute was chosen because it is inert in our operation potential. A Teflon jar containing 200 mL of the buffer solution was used as an electrochemical cell. A three-electrode configuration was adopted. Our photoanode was the working electrode. A Silver/silver chloride(Ag/AgCl) reference electrode (Pine Instrument) and a platinum wire counter electrode were used (see Figure S1c). The three electrodes were connected to a potentiostat (DY2311, Digi-Ivy, or Reference600, Gamry). This whole setup was placed under a solar simulator (Model 91194, 1300 W Xe source with AM 1.5G filter, Newport Oriel) calibrated to 100 mW cm^{-2} using an NREL-certified silicon reference cell equipped with a BK-7 window. A linear voltage sweep was conducted from cathodic to anodic potential with 50 mV s^{-1} rate. No specialty gas purging or stirring was conducted during the measurement. Figure S1b shows the electrochemical setup. Also, in the Supporting Information is a video showing oxygen evolution from a 10 minutes deposition iron oxide film at pH 12 and 1.69 V vs. RHE.

Additional details of experiments are also available in note S1 of the Supporting Information.

Received: June 23, 2011
Revised: September 28, 2011
Published online: November 30, 2011

Keywords: electrochemistry · photoelectrodes · semiconductors · silicon · water oxidation

[1] W. McDowall, M. Eames, *Int. J. Hydrogen Energy* **2007**, *32*, 4611–4626; J. C. van Dyk, M. J. Keyser, M. Coertzen, *Int. J. Coal Geol.* **2006**, *65*, 243–253.
[2] M. Grätzel, *Nature* **2001**, *414*, 338–344; R. M. Navarro Yerga, M. C. A. Galvan, F. del Valle, J. A. V. de La Mano, J. L. G. Fierro, *ChemSusChem* **2009**, *2*, 471–485.
[3] R. van de Krol, Y. Q. Liang, J. Schoonman, *J. Mater. Chem.* **2008**, *18*, 2311–2320.
[4] M. W. Kanan, D. G. Nocera, *Science* **2008**, *321*, 1072–1075.
[5] Y. J. Hwang, A. Boukai, P. D. Yang, *Nano Lett.* **2009**, *9*, 410–415; T. Osaka, H. Kitayama, N. Hirota, S. S. Eskildsen, *Electrochim. Acta* **1984**, *29*, 1365–1370; H. Morisaki, H. Ono, H. Dohkoshi, K. Yazawa, *Jpn. J. Appl. Phys.* **1980**, *19*, L148–L150; G. Nogami, H. Yamaguchi, G. Maeda, K. Beppu, Y. Ueda, T. Nakamura, *J. Appl. Phys.* **1983**, *54*, 1605–1609.
[6] S. Licht, B. Wang, S. Mukerji, T. Soga, M. Umeno, H. Tributsch, *J. Phys. Chem. B* **2000**, *104*, 8920–8924; R. E. Rocheleau, E. L. Miller, A. Misra, *Energy Fuels* **1998**, *12*, 3–10; J. J. H. Pijpers, M. T. Winkler, Y. Surendranath, T. Buonassisi, D. G. Nocera, *Proc. Natl. Acad. Sci. USA* **2011**, DOI: 10.1073/pnas.1106545108.
[7] C. J. Sartoretti, B. D. Alexander, R. Solarska, W. A. Rutkowska, J. Augustynski, R. Cerny, *J. Phys. Chem. B* **2005**, *109*, 13685–13692; E. Thimsen, F. Le Formal, M. Gratzel, S. C. Warren, *Nano Lett.* **2011**, *11*, 35–43.
[8] M. D. Merrill, R. C. Dougherty, *J. Phys. Chem. C* **2008**, *112*, 3655–3666.
[9] Y. S. Hu, A. Kleiman-Shwarsctein, G. D. Stucky, E. W. McFarland, *Chem. Commun.* **2009**, 2652–2654; J. A. Glasscock, P. R. F. Barnes, I. C. Plumb, N. Savvides, *J. Phys. Chem. C* **2007**, *111*, 16477–16488.
[10] J. Brillet, M. Gratzel, K. Sivula, *Nano Lett.* **2010**, *10*, 4155–4160.
[11] K. J. Kim, D. W. Moon, S. K. Lee, K. H. Jung, *Thin Solid Films* **2000**, *360*, 118–121.
[12] X. S. Ye, D. S. Lin, Z. K. Jiao, L. D. Zhang, *J. Phys. D* **1998**, *31*, 2739–2744; A. A. Akl, *Appl. Surf. Sci.* **2004**, *233*, 307–319; Y. L.

Hou, Z. C. Xu, S. H. Sun, *Angew. Chem.* **2007**, *119*, 6445 – 6448; *Angew. Chem. Int. Ed.* **2007**, *46*, 6329 – 6332.
[13] S. W. Boettcher, J. M. Spurgeon, M. C. Putnam, E. L. Warren, D. B. Turner-Evans, M. D. Kelzenberg, J. R. Maiolo, H. A. Atwater, N. S. Lewis, *Science* **2010**, *327*, 185 – 187; B. M. Kayes, H. A. Atwater, N. S. Lewis, *J. Appl. Phys.* **2005**, *97*, 11.
[14] R. Brimblecombe, G. C. Dismukes, G. F. Swiegers, L. Spiccia, *Dalton Trans.* **2009**, 9374 – 9384.
[15] M. Dinca, Y. Surendranath, D. G. Nocera, *Proc. Natl. Acad. Sci. USA* **2010**, *107*, 10337 – 10341.
[16] S. D. Tilley, M. Cornuz, K. Sivula, M. Gratzel, *Angew. Chem.* **2010**, *122*, 6549 – 6552; *Angew. Chem. Int. Ed.* **2010**, *49*, 6405 – 6408; S. U. M. Khan, J. Akikusa, *J. Phys. Chem. B* **1999**, *103*, 7184 – 7189.
[17] S. R. Morrison, *Electrochemistry at semiconductor and oxidized metal electrodes*, Plenum press, New York, **1980**.
[18] M. J. Madou, B. H. Loo, K. W. Frese, S. R. Morrison, *Surf. Sci.* **1981**, *108*, 135 – 152.

